CHAPTER IV
RESULTS AND DISCUSSION

4.1 Characterization of Organophilic-Clay

4.1.1 FTIR

The chemical characteristics of both the organic and inorganic materials can be studied by IR spectra analysis. Figure 4.1 (a) shows the FTIR spectra of dodecylamine-montmorillonite compared with (b) dodecylamine and (c) sodium-montmorillonite. The FTIR spectrum of dodecylamine-montmorillonite shows the specific absorption characteristics of both inorganic and organic components with respect to the alumino-silicate layers and the alkylammonium molecules. The inorganic clay component shows a band at 1050 cm^{-1} which can be associated with Si-O stretching, and those between 600 and 400 cm^{-1} with Al-O stretching and Si-O bending. The dodecylamine component shows bands at 2920, 2850, 1460, and 1370 cm^{-1} which can be assigned to $-CH_2-$, $-CH_3$ stretching and bending, respectively. The FTIR spectrum of dodecylamine-montmorillonite also exhibits a new absorption band at 3012 cm^{-1}which can be assigned to symmetric and asymmetric stretching of $R-NH_3^+$ group. The band indicates that the organophilic cations react with the alumino-silicate layers of montmorillonite.

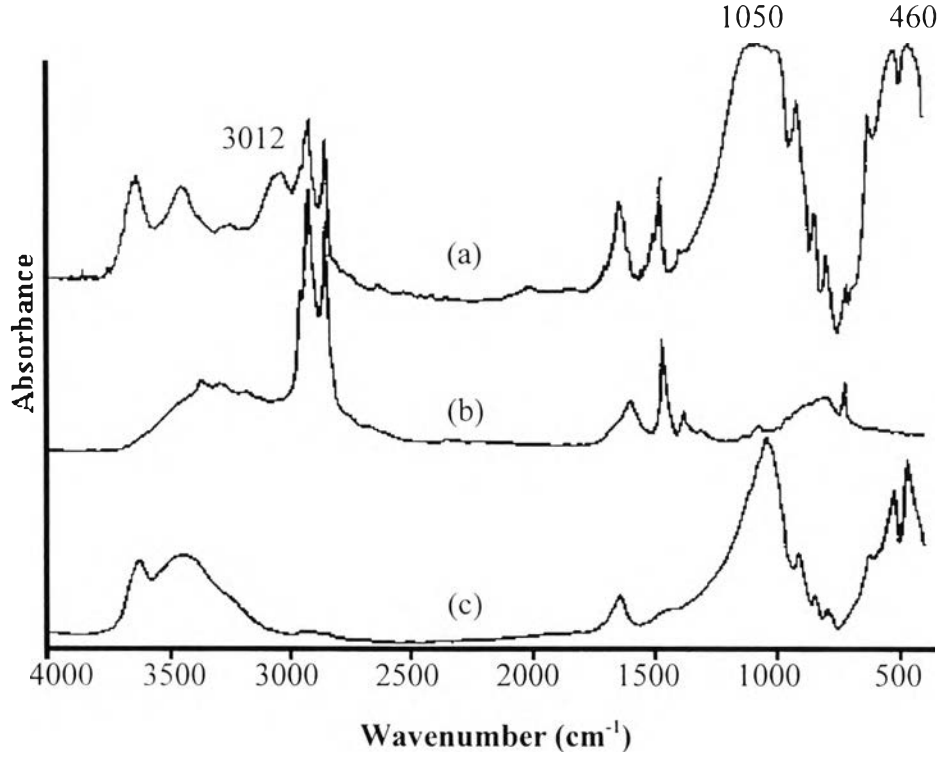

Figure 4.1 The FTIR spectra of (a) dodecylamine-montmorillonite (b) dodecylamine and (c) sodium-montmorillonite.

As seen the IR spectra of Figure 4.1, all assignments of dodecylamine-montmorillonite, dodecylamine and sodium-montmorillonite are summarized in Table 4.1, 4.2 and 4.3, respectively.

Table 4.1 The FTIR absorption bands assignment of dodecylamine-montmorillonite

Frequencies (cm^{-1})	Assignments
3630	-OH stretching
3440	-OH stretching (dimers)
3350 and 3290	N-H stretching of primary amine
3012	symmetric and asymmetric stretching of R-NH_3^+ group
2920	-CH_2- aliphatic chains
2850	-CH_3 stretching
1600	symmetric N-H bending
1460	-CH_2- bending
1370	-CH_3 bending
1050	Si-O stretching
1010	C-N stretch in aliphatic amine
720	N-H out of plane bending
520	Al-O stretching
460	Si-O bending

Table 4.2 The FTIR absorption bands assignment of dodecylamine

Frequencies (cm^{-1})	Assignments
3360 and 3290	N-H stretching of primary amine
2920	$-CH_2-$ aliphatic chains
2850	$-CH_3$ stretching
1597	symmetric N-H stretching
1470	$-CH_2-$ bending
1380	$-CH_3$ bending
1010	C-N stretching in aliphatic amine
720	N-H out of plane (OOP) bending

Table 4.3 The FTIR absorption bands assignment of sodium-montmorillonite

Frequencies (cm^{-1})	Assignments
3620	-OH stretching
3440	-OH stretching (dimers)
1040	Si-O stretching
520	Al-O stretching
466	Si-O bending

4.1.2 WAXS

The Wide Angle X-ray Scattering (WAXS) patterns of sodium-montmorillonite and dodecylamine-montmorillonite in the region between $2\theta = 3°$ and $2\theta = 10°$ are shown in Figure 4.2 (a) and (b). Each curve shows only one peak, i.e. at $2\theta = 7.2°$ and $2\theta = 5.0°$, respectively. The peaks can be assigned to the 001 lattice spacing of silicate layer in montmorillonite as suggested by Usuki et al. (1993). The interlayer spacing corresponding to these peaks increases from 12.26 Å to 17.90 Å as described in Figure 4.3. The WAXS results are in agreement with the basal spacing of alumino-silicate layer using an ω-amino acid as an organic cation (Okada and Usuki, 1995).

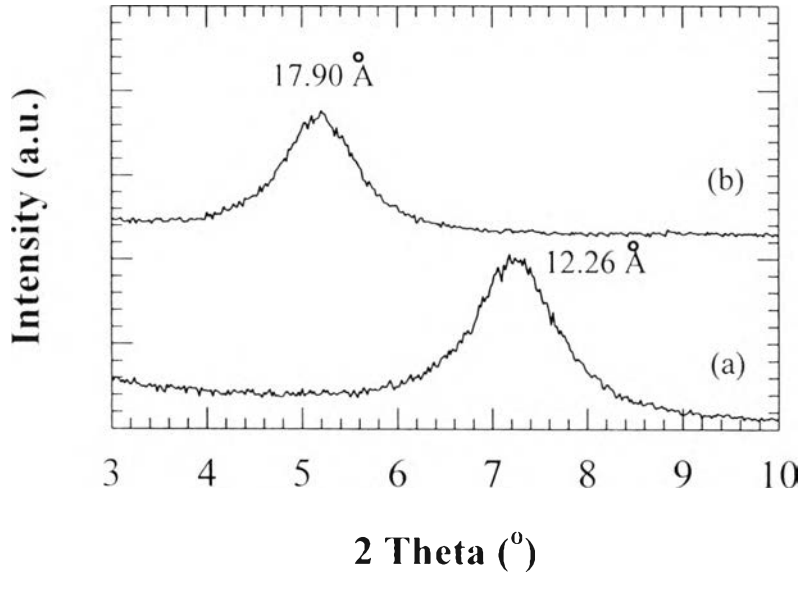

Figure 4.2 The WAXS pattern of (a) sodium-montmorillonite and (b) dodecylamine-montmorillonite.

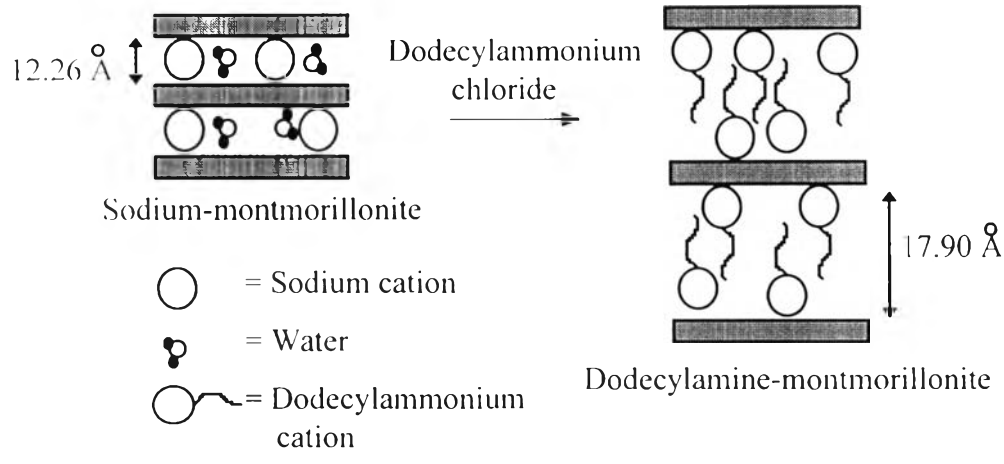

Figure 4.3 A schematic diagram describing the basal spacing between alumino-silicate layers of montmorillonite.

4.1.3 TGA

The thermal stability of the organophilic-clay and the sodium-montmorillonite were determined by thermogravimetric analysis. Figure 4.4 shows the thermograms of sodium-montmorillonite, dodecylamine, and dodecylamine-montmorillonite. For the sodium-clay , the sample shows a slight decrease at 80 °C. This may be attributed to the evaporation of absorbed water in the sample. Above 593 °C, a slight weight loss occurs due to a decomposition of some inorganic materials, as shown in Figure 4.4 (a). For dodecylamine, the sample shows a dramatic decomposition at temperature of 185 °C, as shown in Figure 4.4 (b). For the dodecylamine-clay, a slight weight loss can be observed at the temperature of 200 °C. The sample decomposes significantly at temperature of 340 °C, as seen in Figure 4.4 (c). Thus, it is indicated that dodecylammonium ions react with clay. The thermogram of the dodecylamine-clay also shows the absence of evaporation of absorbed water at 80 °C.

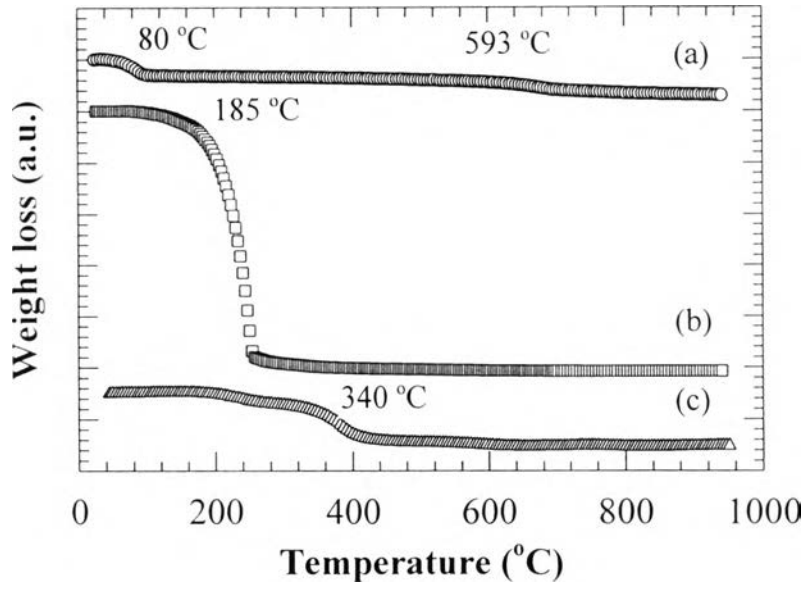

Figure 4.4 The decomposition behaviors of (a) sodium-montmorillonite (b) dodecylamine and (c) dodecylamine-montmorillonite.

4.1.4 AAS

The purity of the organophilic-montmorillonite was determined by measuring a recovery percentage of sodium ions in an acidic solution. Table 4.4 shows the mean value of sodium ions recovery from sodium-montmorillonite and dodecylamine-montmorillonite as measured by the air-acetylene flame AAS (see determination method in appendix II). The recovery percentage of sodium ions in this experiment shows a significant reduction from 2.87 % weight in sodium-clay to 0.21 % weight in organophilic-clay. The percentage conversion of organophilic-clay from sodium-clay can be calculated by the expression

$$\% \text{ Conversion} = \frac{(\text{Na}^+ \text{ in sodium-mont.} - \text{Na}^+ \text{ in DDM-mont.})}{(\text{Na}^+ \text{ in sodium-montmorillonite})} \times 100 \quad \textbf{(4.1)}$$

The dodecylamine-montmorillonite as produced by 1 : 1 in mole ratio of montmorillonite and organic cation yields the average value of 93 % in conversion.

Table 4.4 The mean value of recovery percentage of sodium ions as measured by Atomic Absorption Spectrometry (AAS)

Species	Sodium-clay	Dodecylamine-clay
Na^+ (%wt)	2.87* $\pm$ 0.02	0.21 $\pm$ 0.01

* The exact value from Kunimine 's technical data sheet is 3.15 % weight.

4.2 Characterization of Polyimide-Clay Nanocomposite Thin Films

4.2.1 FTIR

The FTIR spectroscopy can be used to characterize the chemical characteristics of the nanocomposite thin films. Figure 4.5 and Figure 4.6 show the specular reflectance FTIR spectra of BPDA/PDA (PI2610) and BTDA/ODA-MDA (PI2579) polyimide films with various of clay contents in the nanocomposite films and the spectrum of the organophilic-montmorillonite.

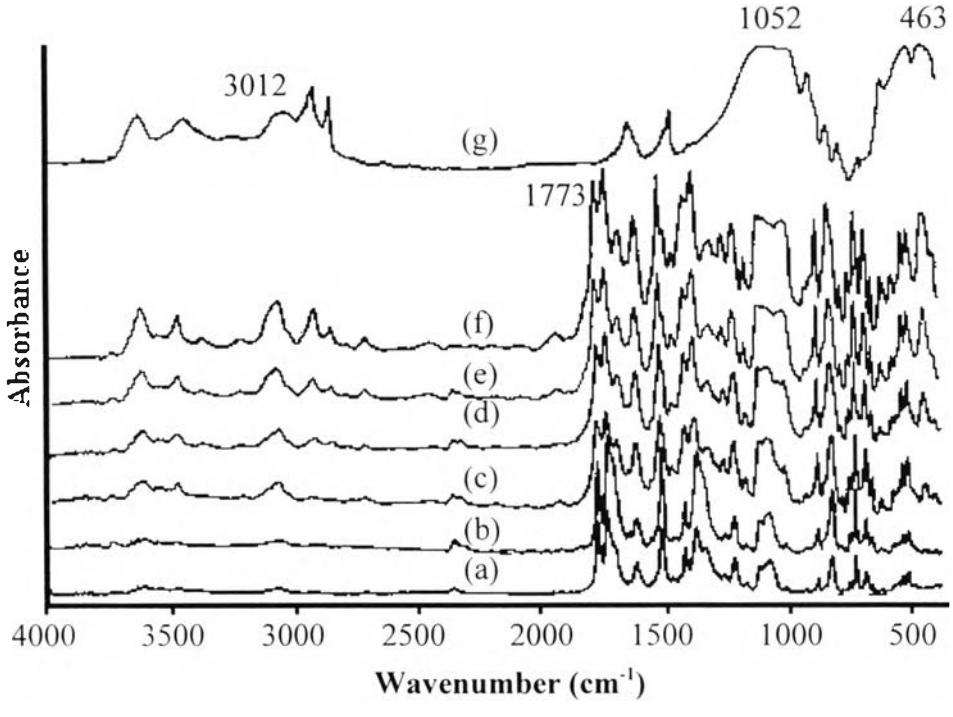

Figure 4.5 The specular reflectance FTIR spectra of (a) BPDA/PDA polyimide (b) polyimide-clay 1 % wt (c) 3 % wt (d) 6 % wt (e) 9 % wt (f) 11 % wt and (g) dodecylamine-montmorillonite.

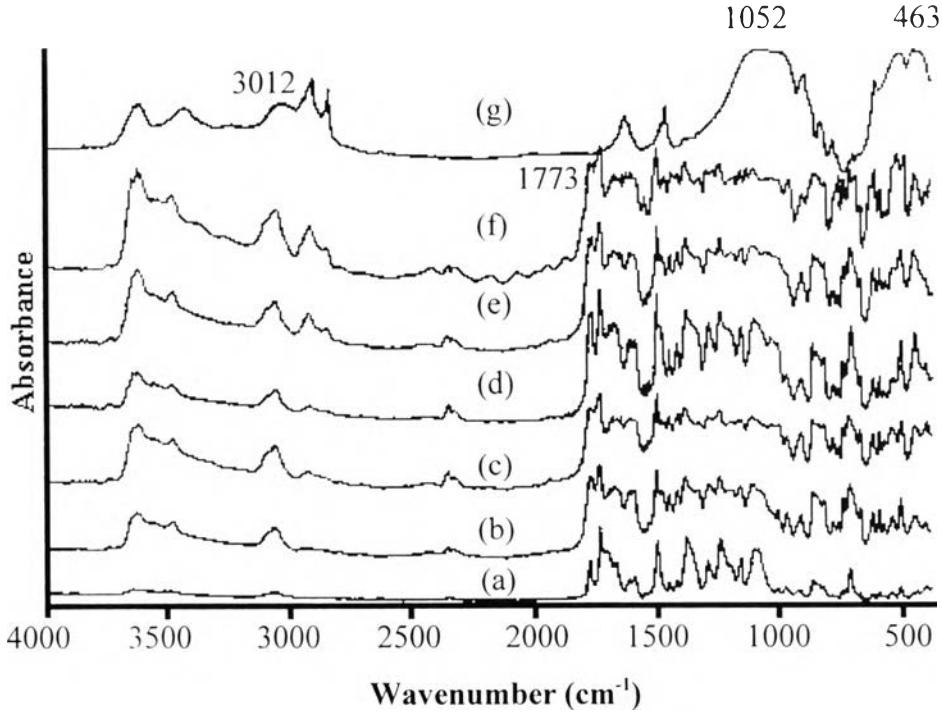

Figure 4.6 The specular reflectance FTIR spectra of (a) BTDA/ODA-MDA polyimide (b) polyimide-clay 1 % wt (c) 3 % wt (d) 6 % wt (e) 9 % wt (f) 11 % wt and (g) dodecylamine-montmorillonite.

The FTIR spectra of the polyimide-clay nanocomposites as shown in Figures 4.5 and 4.6 (b)-(f) indicate the absorption characteristics of both organic and the specific filler component. The bands at 1050 and 460 cm^{-1} can be assigned to Si-O stretching and bending from the alumino-silicate layers. The band at 1773 cm^{-1} can be associated with the symmetric stretching of carbonyl absorption (C=O) in imide groups. All of these increase with increasing clay content. The polyimide-clay nanocomposite films also display the frequency of $R\text{-}NH_3^+$ at 3012 cm^{-1}. This may result from the terminal group of organic cations in the organophilic-clay or polyimide molecules react with the alumino-silicate layers of the particular filler. The absorption bands as shown in the range of 3700-3200 cm^{-1} are associated with free or hydrogen-bonded -OH stretching. This may result from either the absorbed water in the film or the hydroxyl groups in silicate layers of a montmorillonite. All of the nanocomposite films show an important wide band in this region but this band is insignificant for an ordinary polyimide film.

4.2.2 WAXS

Figure 4.7 shows the WAXS pattern of BPDA/PDA polyimide and its clay nanocomposite films. All of the films display a broad band in the region between $2\theta \approx 15°$ and $2\theta \approx 30°$. The band suggests that the films contain amorphous regions or partially ordered structures. The WAXS patterns of the nanocomposite also show a sharp peak at $2\theta = 6.4°$ and no sharp reflections below $2\theta = 3°$. A sharp peak can be related to an interlayer spacing of the natural sodium-montmorillonite, i.e. 13.77 Å. These two characteristics of the nanocomposite film reveal that some of the alumino-silicate layers produce fine dispersion as a single layer and some of them are close together as a stacked-layer. In addition, the BPDA/PDA polyimide-clay nanocomposite can be classified as a partial-exfoliated nanocomposite which

is a particular type of the clay composites as described by Pinnavaia et al. (1996). The model of this system is illustrated in Figure 4.8.

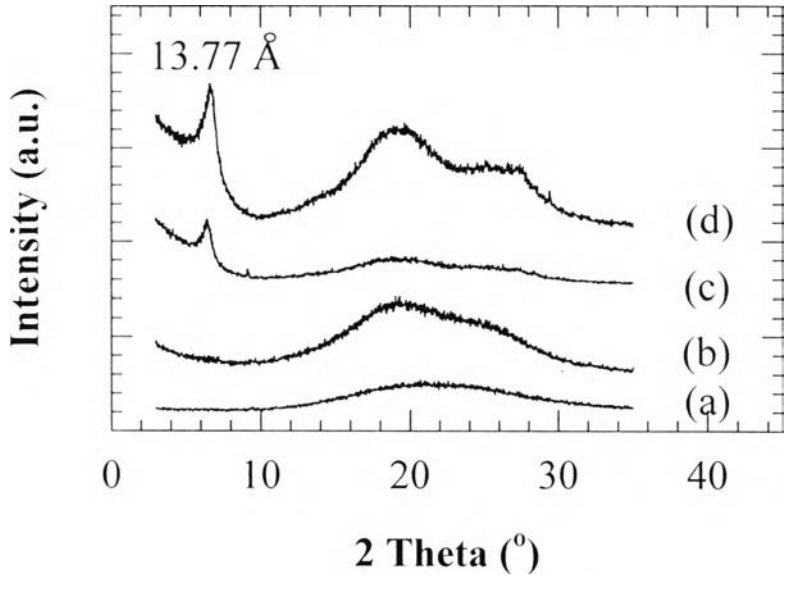

Figure 4.7 The WAXS pattern of (a) BPDA/PDA polyimide film (b) polyimide-clay 0.5 % wt (c) 6 % wt and (d) 9 % wt.

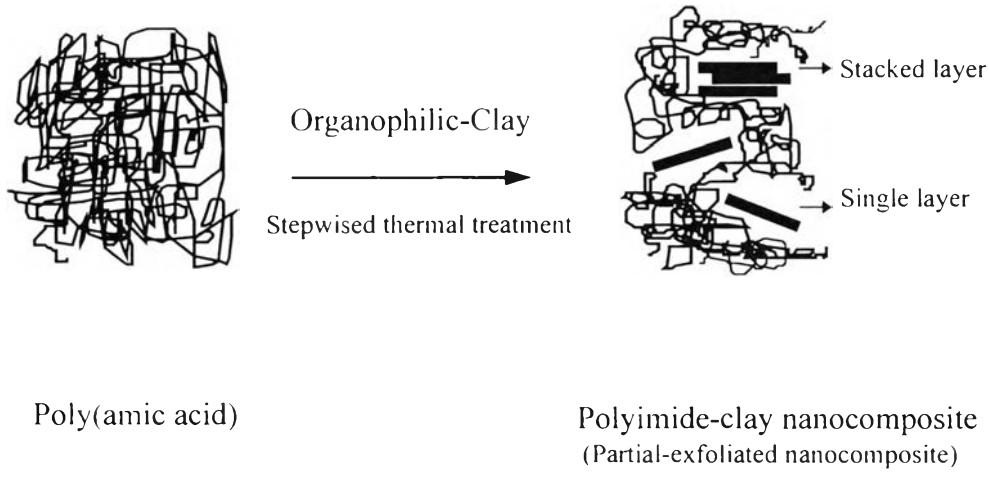

Figure 4.8 The possible model for BPDA/PDA polyimide-clay nanocomposite thin film.

4.2.3 TGA

The thermogravimetric analysis results of BPDA/PDA polyimide-clay nanocomposite films show that the thermal stability tends to improve with increasing organophilic-clay content as shown in Figure 4.9 (see also appendix III). The degradation temperature of BPDA/PDA polyimide-clay nanocomposites exhibit a significant increment by as much as 30 °C relative to an untreated polymer. This may result from the hydrophobic interaction between the polyimide chain and alumino-silicate layer of the filler. The polymer chains probably need an additional amount of thermal energy to destroy this specific interaction, so the inorganic filler can delay the thermal degradation of the polymeric material.

The final residue at 950 °C is a further information that can be obtained from the TGA. All of them contain a mixture of white silica and black char powder. The contents of silica and black char residues vary with the amount of organic polymer and the particular filler, i.e. the white silica residue would be increased with the increase of the organophilic-clay content.

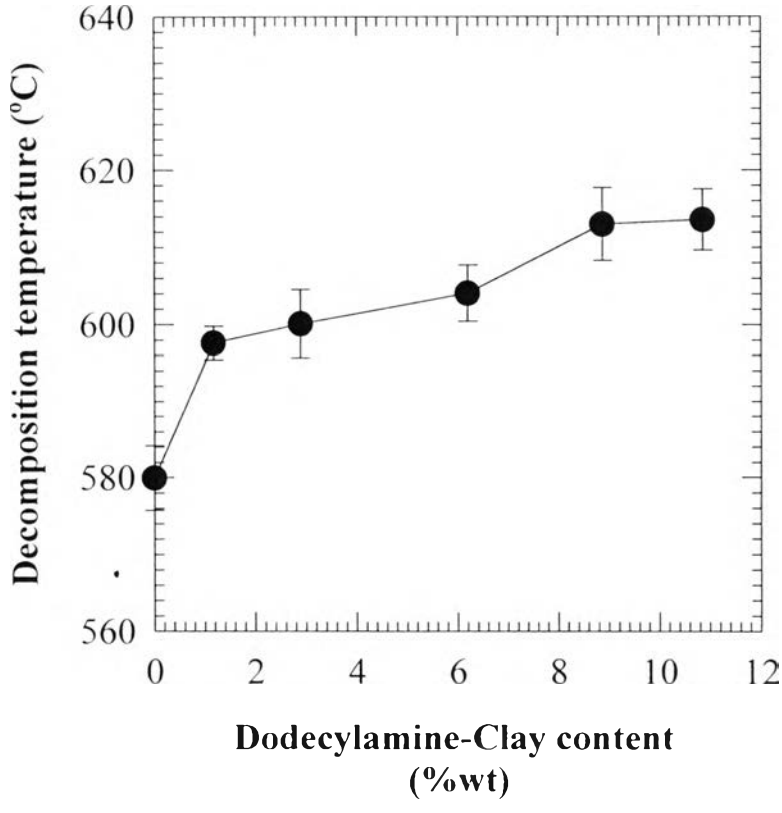

Figure 4.9 Effect of organophilic-clay on decomposition temperature of BPDA/PDA polyimide film.

4.2.4 TEM and SAED

The structural characterization of the polyimide-clay nanocomposite films was obtained by Transmission Electron Microscopy (TEM) and Selected Area Electron Diffractometry (SAED). Figure 4.10 shows transmission electron micrographs of various clay contents in BPDA/PDA polyimide-clay nanocomposites. The individual alumino-silicate layer shows a dark line with a 2000 Å in average length. These layers produce

fine dispersion and become more closer as the amount of organophilic-clay increases. Additionally, the large amount of organophilic-clay in the nanocomposites exhibits many aggregated-layers and poorer dispersion of organophilic-clay as shown in Figure 4.10 (b) and (c). This may result from many of unreacted alumino-silicate layers which are stacked close together. However, the information obtained from TEM images support the WAXS results and confirm a possible model as already illustrated in Figure 4.8.

Figure 4.11 shows the SAED images of various clay contents in BPDA/PDA polyimide-clay nanocomposites. All images exhibit unclear continuous rings. These reveal that the nanocomposites are, as a whole, in form of amorphous with the fine dispersion of alumino-silicate layers in the polymer matrix. In addition, all of these information can support the WAXS patterns resulting in a partial-nanocomposite.

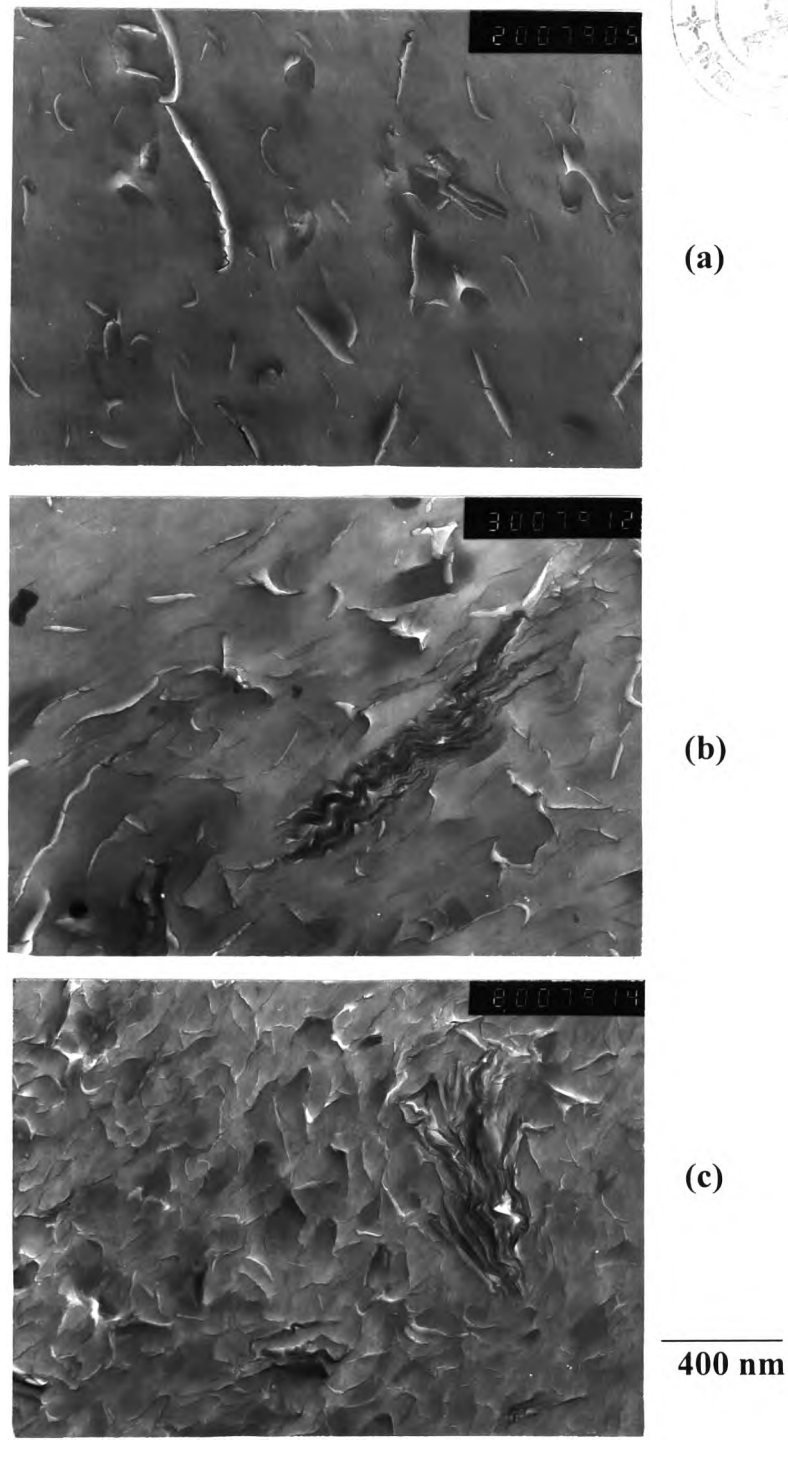

Figure 4.10 Transmission electron micrographs of (a) BPDA/PDA polyimide-clay 1 % wt (b) 6 % wt and (c) 9 % wt.

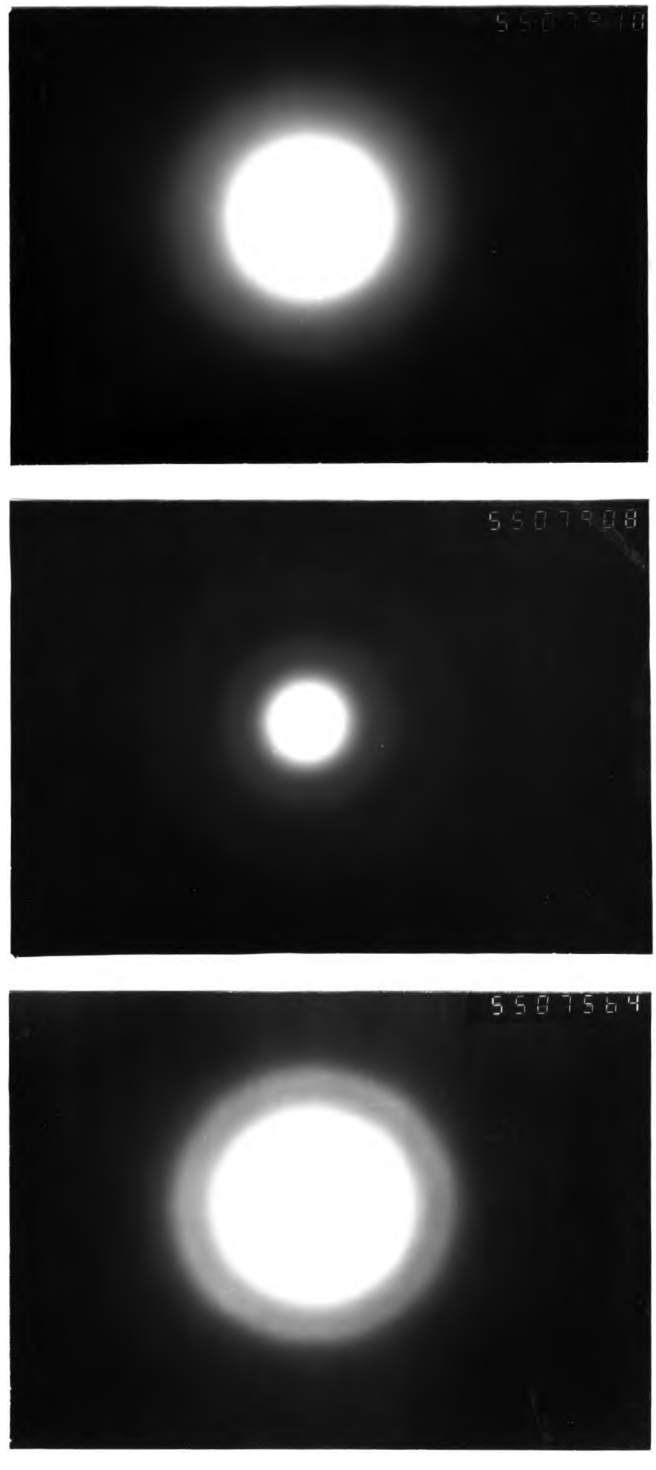

Figure 4.11 Selected area electron diffraction images of (a) BPDA/PDA polyimide-clay 1 % wt (b) 6 % wt and (c) 9 % wt.

4.3 Properties Measurements

4.3.1 In-Plane CTE (α_{xy})

The thermal expansion coefficient (CTE) is an important parameter for protective coating applications in microelectronics devices, since many times of thermal operation in the material can induce stress-developments as described by Pottiger et al. (1994). Typically, the CTE of polymeric materials allows variations with the temperature, such as the CTE of a hand-coated rigid-rod polyimide film (PI2610) as shown in Figure 4.12. A slight increment of the CTE with temperatures can be observed from the beginning until 320 °C, where the specimen starts to expand drastically. The onset point in the curve corresponds to an expansion temperature (T_e). Because the CTE of material varies with temperature, an average value over a specified temperature range, e.g. 50-250 °C is quoted instead.

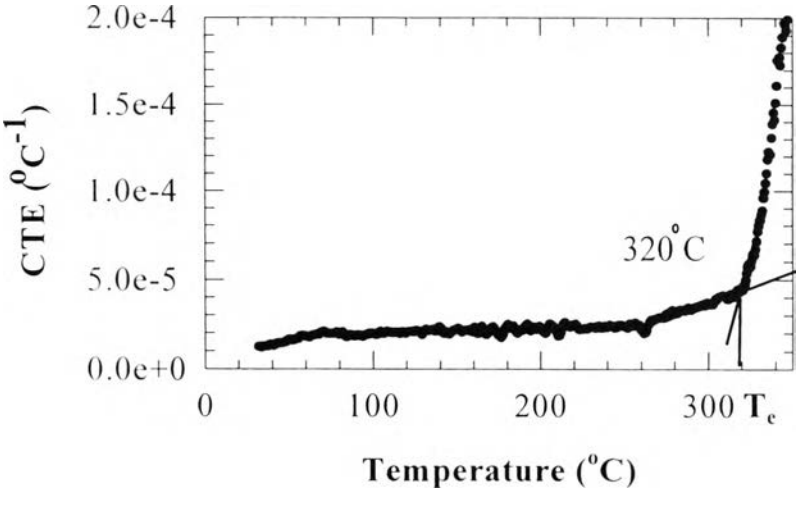

Figure 4.12 The temperature dependence of an in-plane CTE of BPDA/PDA polyimide film.

Table 4.5 shows the in-plane CTE results of BPDA/PDA and BTDA/ODA-MDA polyimide films with their expansion temperature (T_e) and yielding temperature (T_y) (see appendix IV). The in-plane CTE of the films was determined over the temperature range between 50 to 250 °C with roughly 25 μm in average thickness.

Table 4.5 The in-plane CTE results with expansion and yielding temperature of BPDA/PDA (PI2610) and BTDA/ODA-MDA (PI2579) polyimide films

Materials	$\alpha_{50\text{-}250}$ (ppm/°C)	T_e(°C)	T_y(°C)
PI2610, rigid-rod	39.48	326	365
PI2579, flexible	70.02	302	312

The results in Table 4.5 show that more rigid rod-like in the chain structure, the lower the in-plane CTE value becomes. The possible explanation of the difference in CTE was described by Numata et al. (1986). The rigid-rod polyimide chains usually arrange themselve in the planar axis since their skeleton contain many benzene rings with no heteroatom in group VI, i.e. oxygen or sulphur, linkages. This conformation will be expanded very little when temperature is raised. In contrast, the flexible polyimide will lose its conformation because it contains many ether (-o-) linkages and resulting in a zigzag conformation. The zigzag conformation can be easily expanded when temperature is increased. The conformation of rigid-rod and flexible polyimide chains are showed in Figure 4.13. The result as shown in Table 4.3 also shows that the more rigid rod-like the chains, the lower the expansion and yielding temperatures become because the polymer chains are difficult to

move. This may result from the more closer arrangement of the rigid-rod polymer chains than the flexible one.

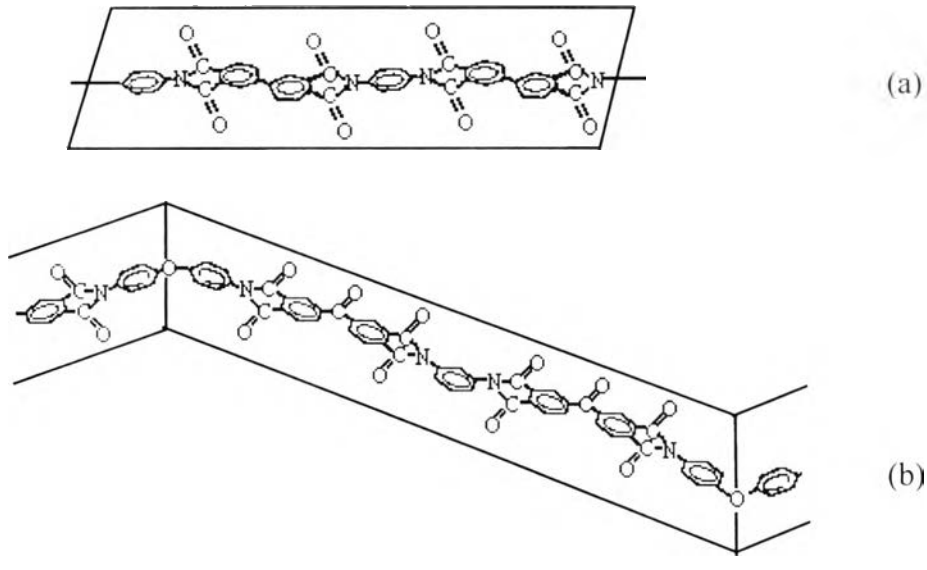

Figure 4.13 The conformation of (a) rigid-rod and (b) flexible polyimide chains.

Many researchers have studied the relationship between the CTE and the other controlling factors of the polyimide films. Jou et al. (1992) found that the CTE increases with film thickness. Jou et al. (1991) and Asawakanjana (1997) investigated the effect of curing conditions on the CTE of the film. The result revealed that higher curing temperature can reduce the CTE.

Figure 4.14 shows effect of the organophilic-clay content on the in-plane CTE of both rigid-rod (BPDA/PDA) and flexible (BTDA/ODA-MDA) polyimide films. The results are in agreement with the previous work of Yano et al. (1993) who determined effect of the same clay on the in-plane CTE of PMDA/ODA polyimide film. The CTE improvements may result from a fine dispersion of alumino-silicate layers in the polymer matrices and

the rigidity of this inorganic filler can suppress the expansion of polymer chains when temperature is raised. However, it is noted that all of treated polyimides still have higher CTE as compared to that of the silicon substrate which has the average CTE in the range of 2-4 ppm/°C.

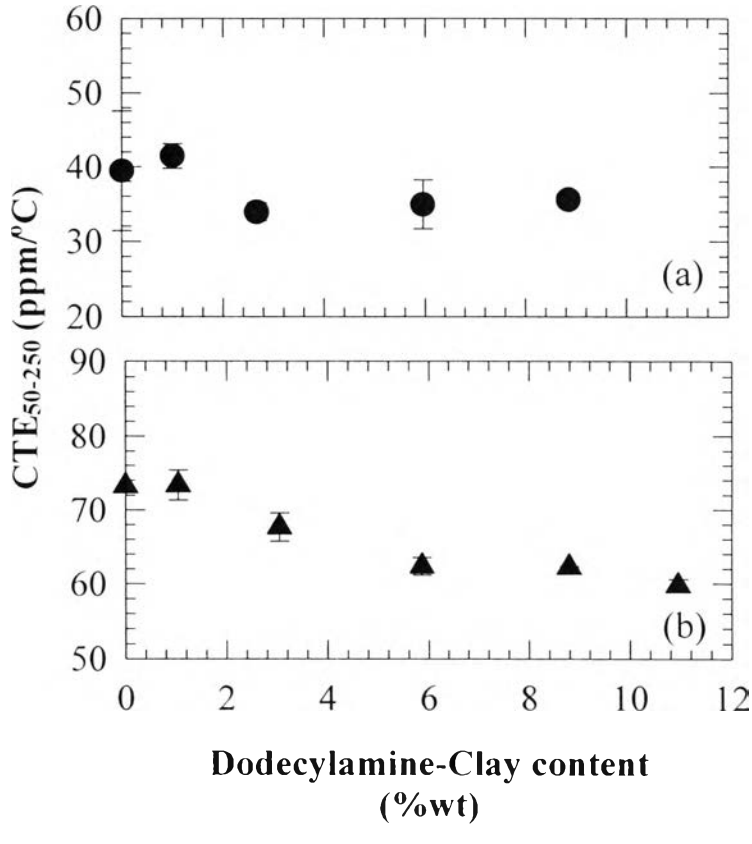

Figure 4.14 Effect of the organophilic-clay content on the in-plane CTE of (a) BPDA/PDA-clay nanocomposites and (b) BTDA/ODA-MDA-clay nanocomposites.

Figure 4.15 shows effect of the organophilic-clay content on expansion temperature (T_e) of both rigid-rod and flexible polyimide films.

The T_e of polyimide-clay nanocomposite films shows a slight reduction for all contents of clay compared to an ordinary polymer. This indicates that adding more organophilic-clay are hardly effective to hinder the motion of polymer chains. These may result from the aggregation of alumino-silicate layers. Hence, the polymer chain becomes easier to expand.

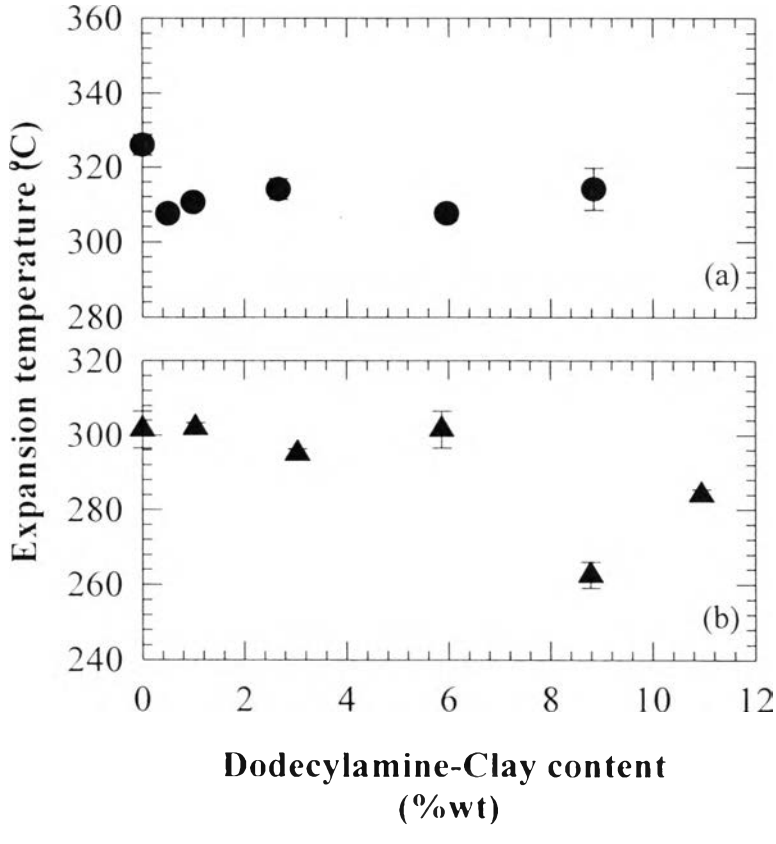

Figure 4.15 Effect of the organophilic-clay content on expansion temperature of (a) BPDA/PDA-clay nanocomposites and (b) BTDA/ODA-MDA-clay nanocomposites.

Table 4.6 shows effect of the organophilic-clay content on yielding temperature (Ty) of both rigid-rod and flexible polyimide films. The PI-Clay as mentioned in the table means polyimide-clay nanocomposite with various clay contents. Adding of organophilic-clay into the rigid rod polyimide can reduce T_y but it cannot be obtained with more clay added. This indicates that the organophilic-clay reducing intermolecular interactions between polymer chains. So, the material becomes more brittle compared to an untreated polyimide. However, it is noted that the organophilic-clay does not affect yielding of flexible polyimide as seen by the T_y showing a nearly constant value relative to an untreated polyimide.

Table 4.6 Effect of the organophilic-clay on yielding temperature of BPDA/PDA (PI2610) and BTDA/ODA-MDA (PI2579) polyimide films

Materials	T_y(°C)	Materials	T_y(°C)
PI2610	365	PI2579	312
PI2610-Clay 0.5 %	324	PI2579-Clay 1.0 %	312
PI2610-Clay 1.0 %	328	PI2579-Clay 3.0 %	312
PI2610-Clay 3.0 %	342	PI2579-Clay 6.0 %	325
PI2610-Clay 6.0 %	-	PI2579-Clay 9.0 %	325
PI2610-Clay 9.0 %	-	PI2579-Clay 11.0 %	319

4.3.2 Effect of Thermal Cycling on In-Plane CTE

The thermal cycling experiment is the other important parameter that can be used as an appropriate protective material for microelectronics devices. This experiment can indicate the dimensional stability during many cycles of temperature changes and can predict the service lifetime of the

testing material. Ten cycles of thermal operation of a rigid-rod polyimide film and its clay nanocomposites were performed, the α_{xy} (in-plane CTE) of each cycle was measured and the results are shown in Figure 4.16 (see also appendix V). The α_{xy} of both rigid-rod polyimide film and its clay nanocomposites allow hardly any changes after ten cycles of heating up and cooling down. All of them give excellent thermal cycling characteristics for the coating applications. However, the material still has to be examined for the other requirements to produce an appropriate protective material.

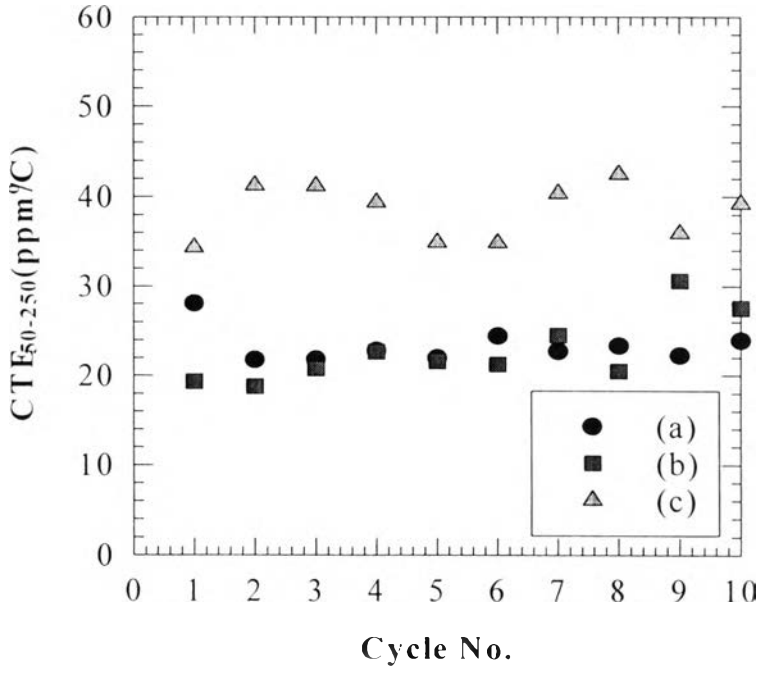

Figure 4.16 Effect of thermal cycling at heating rate of a 5 °C/min on the in-plane CTE of (a) BPDA/PDA polyimide (b) polyimide-clay 1 % wt and (c) 9 % wt.

Figure 4.17 shows the plot of temperature-strain behaviors of a rigid-rod polyimide film and its clay nanocomposites. For ordinary polyimide, the material allows a slow expansion in the first cycle (N=1) resulting in an unsaturated loop. The magnitude of further loops (N>1) become smaller than the former as seen in Figure 4.17 (a). This may result from the reduction of expanded polymer chains because most of them had already expanded along the load direction in the former cycle. The temperature-strain behaviors for small amount of clay in nanocomposite film, which is represented by a 1 % weight of dodecylamine-montmorillonite, also exhibits the same result as well as an ordinary polymer film. This indicates that the greater clay content cannot affect the thermal characteristics of the film. A film of polyimide-clay with 9 % weight shows a small unsaturated loop for the first cycle, but it becomes almost completely closed for further loops. The result reveals that the content of clay is high enough to allow a thermal barrier characteristics and resulting in a thermally reversible material when further thermal energy is applied.

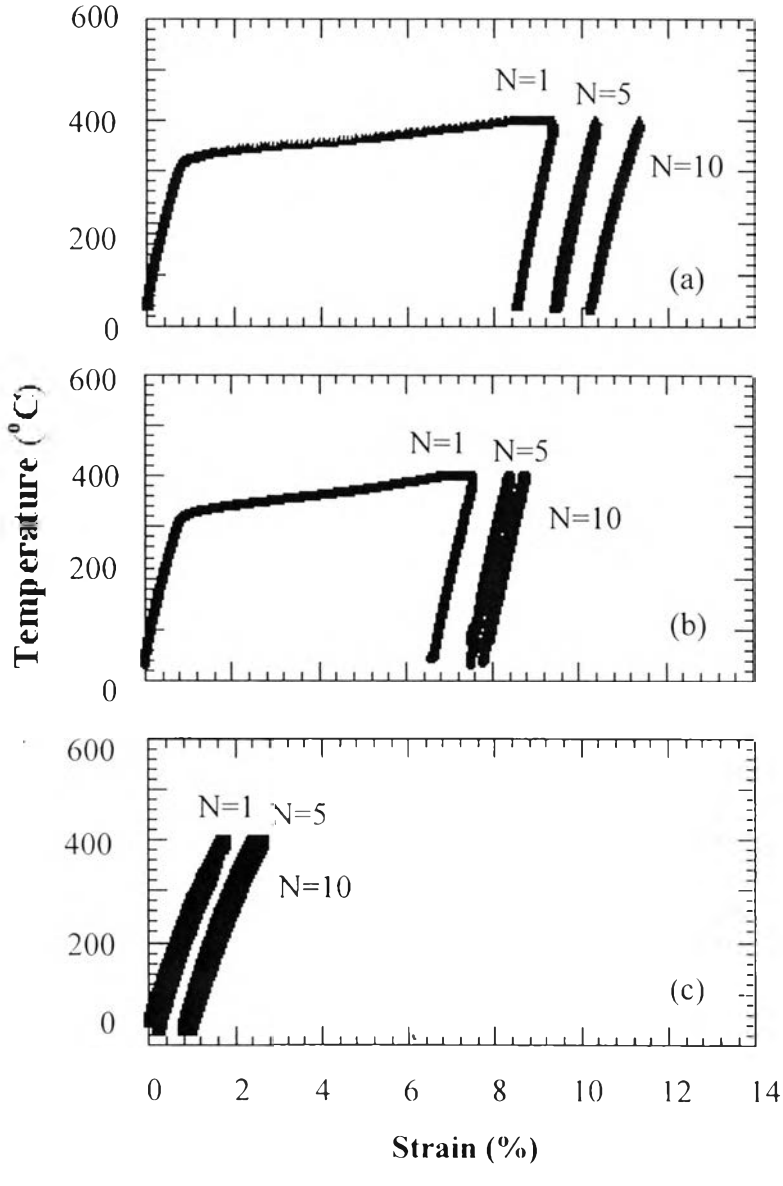

Figure 4.17 The temperature-strain curves of (a) BPDA/PDA polyimide (b) polyimide-clay 1 % wt and (c) 9 % wt.

4.3.3 Ductile-Brittle Characteristics

Typically, the ductile-brittle characteristics of polymeric material at ambient temperature can be determined by using a universal testing machine with an extension mode. The stress-strain curves of BPDA/PDA polyimide film and its clay nanocomposites at 23 °C are presented in Figure 4.18 (see also appendix VI). The tensile properties of each specimen are summarized in Table 4.7.

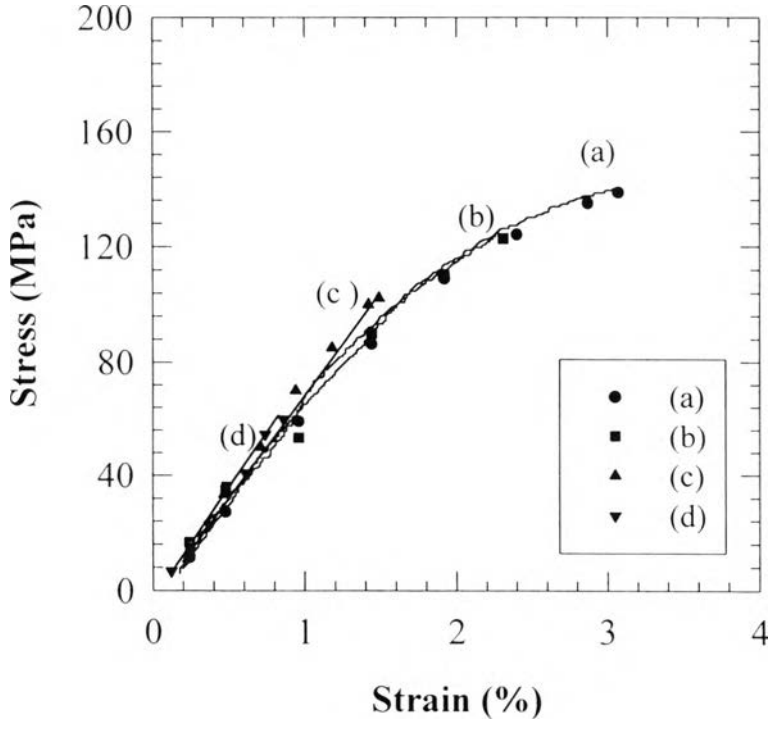

Figure 4.18 Stress-strain curves of (a) BPDA/PDA polyimide film (b) polyimide-clay 0.5 % wt (c) 3 % wt and (d) 8 % wt.

The ordinary rigid-rod polyimide shows a 3 % elongation at break. It decreases with increasing organophilic-clay content. We found

almost 1 % elongation at break for 8 % weight of clay added. This indicates that adding the inorganic filler into a polymeric material can increase brittle characteristics. The results are consistent with the previous studies of Hydroxy polybenzoxazole (HPBO) and Sulfopolybenzobisthazole (SPBT)-silica hybrids as reported by Premachandra et al. (1996). Both systems allowed increase of brittle characteristics as the amount of silica increased. This may result from the rigidity of the inorganic filler. Wang et al. (1994) demonstrated the effect of silica-containing filler on tensile properties of PMDA/ODA polyimide. The result also followed the same trend.

Table 4.7 Tensile properties of BPDA/PDA (PI2610) polyimide film and its clay nanocomposites

Materials	Modulus[a]	Ultimate Strength[b] (GPa)	Ultimate Elongation[c] (%)
PI2610	6.82	4.99	3.02
PI2610-Clay 0.5 %	7.02	4.99	2.35
PI2610-Clay 3.0 %	7.73	6.44	1.57
PI2610-Clay 8.0 %	7.92	6.89	0.94

[a]Initial slope of the stress-strain curve.

[b]Strength at break.

[c]Elongation at break.

The tensile modulus and strength at break of polyimide-clay nanocomposite films show larger increments relative to pure polyimide. The result reveals that the organophilic-clay can act as a reinforcing material for a

polyimide film. However, it is noted that modulus and ultimate strength of PI-Clay 3.0 % and 8.0 %wt are not much different.

4.3.4 Water Absorption

The amount of water absorbed in polymer film can be measured by using thermogravimetric analysis. The water absorption of a rigid-rod polyimide film and its clay nanocomposites is shown in Figure 4.19 (see also appendix VII).

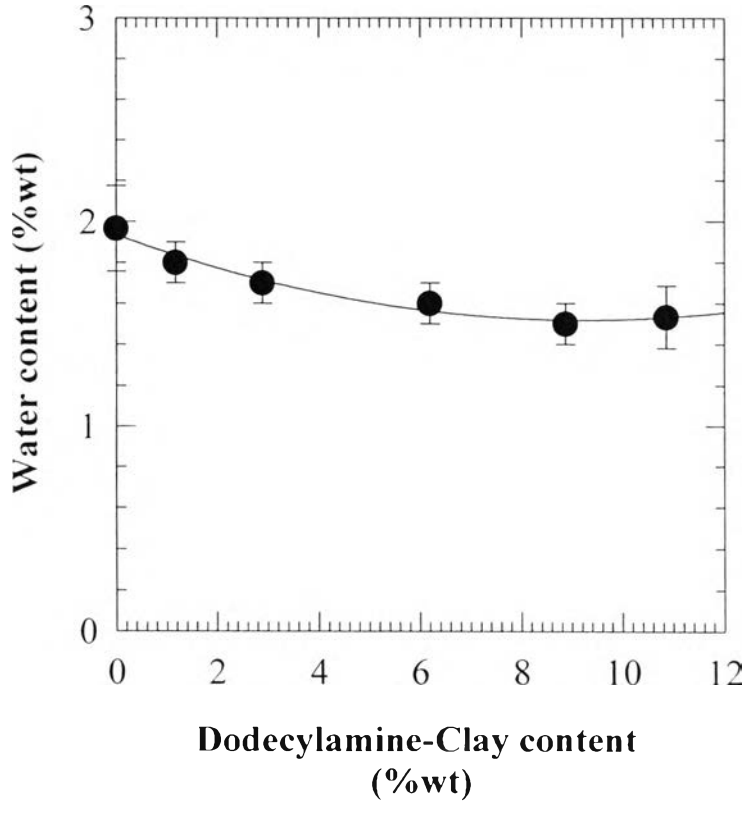

Figure 4.19 Effect of organophilic-clay on water absorption of BPDA/PDA polyimide film.

In general, the water absorption of polyamide and polyimide are very high because the water molecules can easily diffuse to form H-bonding along that polymer chains. But the diffusion of small molecule becomes difficult for the composite which contains a platey or laminated filler as explained by Subramanian et al. (1987) and Kamal et al. (1995). The similar situation was also found in poly(ε-caprolactone)-clay nanocomposite as reported by Messersmith and Giannelis (1995). The reduction of diffusing molecules into the composite may result from the longer tortuous pathway of water molecules as affected by many stacking units of the filler, i.e. the stacking layer can act as a barrier to water diffusion into polymer film. A possible model describing the diffusion of water molecule through polyimide film is shown in Figure 4.20.

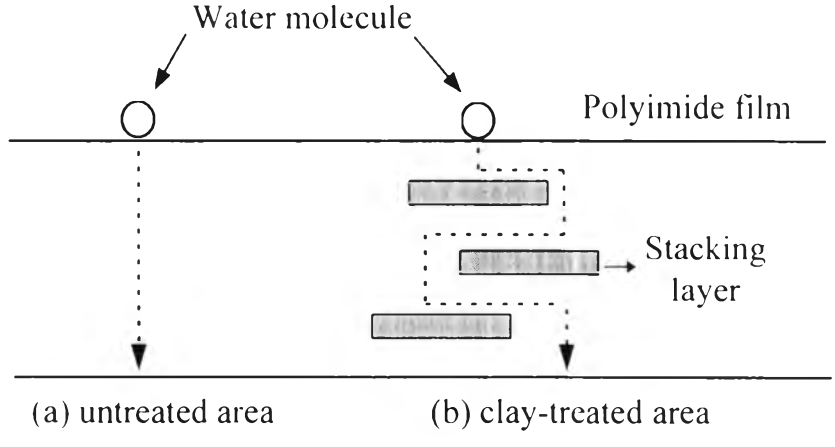

Figure 4.20 A model describing the diffusion of water molecule through polyimide film.

4.3.4 Dielectric Strength

The dielectric strength is an important parameter that can be used to chose an appropriate electrical insulation material. In particular, the dielectric strength is strongly dependent on temperature, specimen thickness,

and humidity. So, most of results are usually reported in a specified testing condition. The dielectric strength of a rigid-rod polyimide film and its clay nanocomposites is shown in Figure 4.21 (see also appendix VIII).

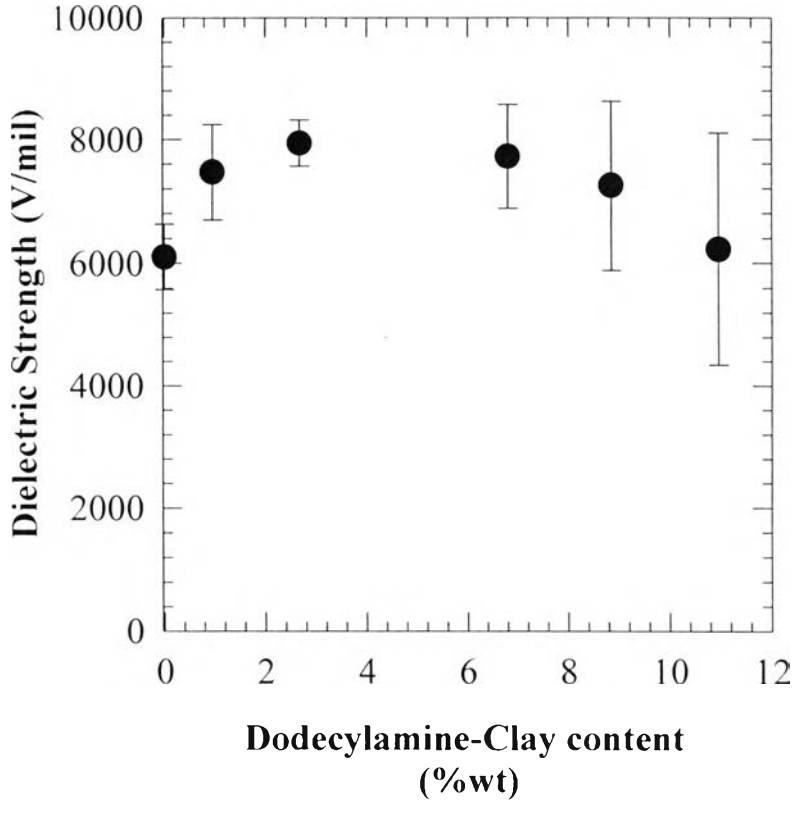

Figure 4.21 Effect of organophilic-clay on dielectric strength of BPDA/PDA polyimide film.

The dielectric strength value of an ordinary rigid-rod polyimide film is consistent with the previous work of Asawakanjana (1997). The clay nanocomposite film with small amount of clay, i.e. less than 3 %wt, shows a slight improvement on dielectric strength value. The similar situation was found in a system of poly(vinyl chloride)-kaolin composite as demonstrated by

Ku and Leipins (1987). The other example was demonstrated by Wade et al. (1993) who reported the improvement of dielectric strength of polypropylene film by adding only 1 % ceresine wax. This composite film showed 40 % increasing in dielectric strength value. Wade suggested that this improvement may result from the filler acts as a nucleating center to trap the high-energy electrons which are generated by the electrodes and dissipate as heat. As a role of filler and close stacking of alumino-silicate layer at high content of clay in rigid-rod polyimide, it may act as impurity in the material that cause some defects to allow electrical treeing growth, the movement of electrical charges through the weakest part of the testing material, and lead to the reduction of dielectric strength with large fluctuations. However, the optimum content of clay is shown at 3 %wt for this measurement.